10308 *Biochemistry* **2009,** *48,* 10308–10320
DOI: 10.1021/bi900980g

BIOCHEMISTRY
including biophysical chemistry & molecular biology
Article

Characterization and Structure of the Manganese-Responsive Transcriptional Regulator ScaR[†,‡]

Kate E. Stoll,[§] William E. Draper,[§] Joseph I. Kliegman,[§,∥] Misha V. Golynskiy,[∥] Rhoda A. T. Brew-Appiah,[§] Rebecca K. Phillips,[§,#] Hattie K. Brown,[§] Wendy A. Breyer,[§] Nicholas S. Jakubovics,[⊥] Howard F. Jenkinson,[⊥] Richard G. Brennan,[#] Seth M. Cohen,[∥] and Arthur Glasfeld*[,§]

[§]*Department of Chemistry, Reed College, Portland, Oregon 97202,* [∥]*Department of Chemistry and Biochemistry, University of California at San Diego, La Jolla, California 92093-0358,* [⊥]*Department of Oral and Dental Science, University of Bristol, Bristol BS1 2LY, U.K., and* [#]*Department of Biochemistry and Molecular Biology, University of Texas M. D. Anderson Cancer Center, Unit 1000, Houston, Texas 77030*

Received June 11, 2009; Revised Manuscript Received September 27, 2009

ABSTRACT: The streptococcal coaggregation regulator (ScaR) of *Streptococcus gordonii* is a manganese-dependent transcriptional regulator. When intracellular manganese concentrations become elevated, ScaR represses transcription of the *scaCBA* operon, which encodes a manganese uptake transporter. A member of the DtxR/MntR family of metalloregulators, ScaR shares sequence similarity with other family members, and many metal-binding residues are conserved. Here, we show that ScaR is an active dimer, with two dimers binding the 46 base pair *scaC* operator. Each ScaR subunit binds two manganese ions, and the protein is activated by a variety of other metal ions, including Cd^{2+}, Co^{2+}, and Ni^{2+} but not Zn^{2+}. The crystal structure of apo-ScaR reveals a tertiary and quaternary structure similar to its homologue, the iron-responsive regulator DtxR. While each DtxR subunit binds a metal ion in two sites, labeled primary and ancillary, crystal structures of ScaR determined in the presence of Cd^{2+} and Zn^{2+} show only a single occupied metal-binding site that is novel to ScaR. The site analogous to the primary site in DtxR is unoccupied, and the ancillary site is absent from ScaR. Instead, metal ions bind to ScaR at a site labeled "secondary", which is composed of Glu80, Cys123, His125, and Asp160 and lies roughly 5 Å away from where the ancillary site would be predicted to exist. This difference suggests that ScaR and its closely related homologues are activated by a mechanism distinct from that of either DtxR or MntR.

Manganese is an essential nutrient for many pathogenic bacteria and has been linked to virulence in a number of species (*1*−*3*). A cofactor for a variety of enzymes involved in fighting oxidative stress, manganese is taken up in bacteria by NRAMP and ABC-type transporters. In streptococci the lipoprotein receptor antigen I (LraI) family of proteins has been linked to infection and has been identified as periplasmic manganese-binding proteins, functioning as a component in ABC transporters. In addition, LraI proteins in streptococcal species are important for virulence and are possible vaccinogens against endocarditis (*3*, *4*). In *Streptococcus gordonii*, an oral bacterium that colonizes the mouth and can cause endocarditis, an LraI homologue plays a role in interbacterial cell adhesion among colonies of oral bacteria (*5*). Referred to as ScaA (for streptococcal coaggregation adherance), it is part of an inducible high-affinity ABC transporter of Mn^{2+} encoded by the *scaCBA* operon (*6*).

The expression of Mn^{2+}-selective ABC transporters in streptococci is under the regulatory control of a group of homologous metalloregulatory proteins, including ScaR[1] from *S. gordonii*, SloR from *Streptococcus mutans*, PsaR from *Streptococcus pneumoniae*, and MtsR from *Streptococcus pyogenes* (*4*, *7*−*9*). They share greater than 50% sequence identity and are either Mn^{2+}-specific or give a mixed response to iron and manganese (*6*, *8*). These regulators are essential to maintaining manganese homeostasis, and loss of the regulator has been shown to impair the virulence of *S. pneumoniae* (*9*). The first member of this group to be characterized, ScaR, selectively represses expression of the *scaCBA* operon in the presence of its corepressor manganese (*7*). Elevation of manganese concentration from 0.1 to 50 μM decreases ScaA production 5-fold. Gel shift assays performed with ScaR and DNA fragments containing the *scaC* promoter region showed that Mn^{2+}, and to a lesser extent Zn^{2+} and Ni^{2+}, activates ScaR for DNA binding, while Fe^{2+}, Cu^{2+}, and Co^{2+} are less effective at 100 μM concentrations (*7*). ScaR protects a 46 base pair stretch of DNA in the promoter region. Two adjacent binding sites for the repressor, each comprised of inverted repeats, were identified based on sequence alignment to a number of other promoter regions from related operons in streptococcal species (*7*).

[†]This work was supported in part by NIH Grant GM069644 (A.G.), NIH Grant GM059323 (J.D.H.), and Robert A. Welch Foundation Grant G-004 (R.G.B.). Purchase of the isothermal titration microcalorimeter was made possible by NSF Grant CHE-0321336.

[‡]Crystallographic data and coordinates have been deposited in the RCSB Protein Data Bank under the file names 3HRS, 3HRT, and 3HRU.

*To whom correspondence should be addressed. E-mail: glasfeld@reed.edu. Phone: (503) 517-7679. Fax: (503) 788-6643.

[1]Abbreviations: ScaR, streptococcal coaggregation regulator; DtxR, diphtheria toxin repressor; HEPES, 4-(2-hydroxyethyl)piperazine-1-ethanesulfonic acid; IdeR, iron-dependent regulator. Bis-Tris, 1,3-bis-(tris(hydroxymethyl)methylamino)propane; HTH, helix−turn−helix; rmsd, root mean -square deviation; ITC, isothermal titration calorimetry.

 Published on Web 10/01/2009

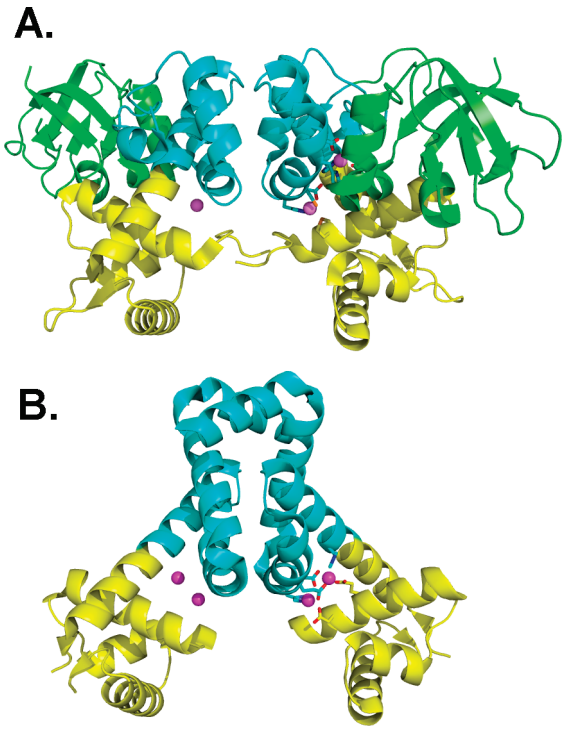

FIGURE 1: Structures of (A) IdeR bound to Co^{2+} (PDB ID 1F57 (*32*)) and (B) MntR bound to Mn^{2+} (PDB ID 2F5D (*16*)). Side chains for metal-binding residues are shown for one subunit of each dimer as are bound metal ions (in pink). The N-terminal, DNA-binding domains are colored yellow, the dimerization domains are in turquoise, and in IdeR the C-terminal domains are colored green.

ScaR and its streptococcal homologues belong to the DtxR/MntR family of metalloregulatory proteins. The namesakes of this family regulate iron (DtxR) and manganese (MntR) uptake in *Corynebacterium diphtheriae* and *Bacillus subtilis*, respectively (*10*, *11*). Both DtxR and MntR are dimers in their active states, but despite similar structures and a number of conserved metal-binding residues in the two proteins, each is activated by metal ions in a distinct manner. DtxR and its closely related homologue, IdeR from *Mycobacterium tuberculosis* (Figure 1), are functional dimers of three-domain subunits that are activated by metal binding to two sites in each subunit 9 Å apart (*12*−*14*). The so-called primary site is located at the interface of the N-terminal DNA-binding domain and the central dimerization domain, and the ancillary site is at the interface of the dimerization domain and a C-terminal domain of unknown function. In contrast, MntR is a two-domain protein, lacking the C-terminal domain found in DtxR, and binds two metal ions 4.4 Å apart, at sites labeled A and C, in a binuclear complex at the interface of the DNA-binding and dimerization domains (Figure 1 (*15*, *16*)). The selectivity of DtxR for iron over manganese derives from ligand selection (*17*). The primary site in DtxR contains two sulfur-containing residues, Met10 and Cys102, while no known proteins selective for Mn^{2+} are known to use sulfur atoms as ligands. In MntR, metal ion selectivity is proposed to derive from coordination geometry of the A site, which appears to select for divalent cations with relatively large ionic radii (*16*). Such binding assists in the formation of the necessary geometry in the C site, allowing the second metal ion to bind and activating MntR for DNA binding. Activated DtxR binds to its cognate DNA sequences as a pair of dimers on opposing faces of the duplex, contacting DNA over a region of approximately 27 base pairs (*18*). Although the interaction of MntR with its cognate DNA sequences is not defined, its cognate operator sequence is roughly 20 base pairs long (*11*).

The origins of specificity of ScaR for its cognate metal ion corepressor and for its operator sequence(s) are unknown. Structurally, ScaR is more similar to the iron regulator, DtxR, than the manganese regulator, MntR. Though sharing only 24% sequence identity, ScaR preserves the three-domain structure of DtxR and many of the metal-binding residues found in DtxR. Yet ScaR is manganese-specific while DtxR in iron-specific (*7*, *17*). Ligand selection may play a role, as the DtxR metal-binding residues Met10 and Cys102 are Asp7 and Glu99 at analogous positions in ScaR. Also, sequence comparisons indicate that ScaR may bind metals in a fashion distinct from DtxR, as two of the ancillary site residues in DtxR, Glu173 and Gln175, do not appear to be present in ScaR. Furthermore, the interaction of ScaR with the *scaC* promoter region appears to be novel within the DtxR/MntR family, with two nonoverlapping recognition sites (*7*). In this work, we present results from crystallographic and solution studies that ScaR binds metal ions and DNA in a different fashion than DtxR or MntR and represents a new subclass of metal-dependent regulators in the DtxR/MntR family.

EXPERIMENTAL PROCEDURES

Expression and Purification of ScaR. The *scaR* gene was amplified from the plasmid pCAL-*scaR* (*7*) by PCR so as to include the three N-terminal residues missing from that construct and to add an *Nde*I restriction site directly to the 5′ end of the gene and a *Hin*d III site directly 3′ to the stop codon. The pCAL-n-EK vector and the PCR product were both digested with *Nde*I and *Hin*dIII, and the two were ligated using T4 DNA ligase to create plasmid pSR2, which harbors the native *scaR* gene under the control of a T7 promoter containing a *lac* operator sequence. Plasmid pSR2 was transformed into *Escherichia coli* BL21(DE3) as an expression host. Cells harboring pSR2 were grown in LB medium containing 100 μg/mL ampicillin at 37 °C. For expression, cells were grown to an OD_{600} of roughly 0.8, and induction was initiated by the addition of IPTG to a final concentration of 1 mM in cultures. Following continued incubation for 2 h, cells were harvested by centrifugation and frozen at −80 °C.

Purification of ScaR proceeded by thawing frozen cells from 2 L of culture and resuspending in buffer A (25 mM HEPES, pH 7.0, and 5% (v/v) glycerol) containing 100 μM PMSF, 50 mM NaCl, 1 mM DTT, and 1 mM EDTA. Bugbuster detergent (10× concentrated; Novagen) was diluted into the suspension, which was incubated for 20 min at room temperature prior to centrifugation to remove insoluble cell debris. The cell lysate was loaded on a DE-53 cellulose column (2.5 × 20 cm; Whatman) and eluted with a 50−750 mM NaCl gradient in 300 mL of buffer A with 1 mM EDTA and 1 mM DTT. Fractions containing ScaR were pooled and dialyzed against buffer A containing 1 mM EDTA, 1 mM DTT, and 150 mM NaCl. The dialyzed solution was then loaded on a CM-Sepharose column (2.5 × 15 cm, Amersham) and eluted with a 50−750 mM NaCl gradient in 300 mL of buffer A. Fractions containing ScaR were pooled and dialyzed against several exchanges of buffer A containing 200 mM NaCl, with the final dialysis containing 10 g/L Chelex resin (Bio-Rad). Protein to be used in fluorescence anisotropy and isothermal calorimetric titrations was dialyzed against buffer B (25 mM HEPES, pH 8.0, 500 mM NaCl, and 10% (v/v) glycerol) also containing 10 g/L Chelex resin. Following concentration, protein solutions were flash-cooled in liquid nitrogen and stored at −80 °C.

Table 1: Sequence of the *scaC* Promoter Region and 5′-Fluoresceinated Oligonucleotides Used in This Study[a]

name	sequence	K_d (nM)
scaC	**AAAATTAACTTGACTTAATTTT***TATGTTAAGGTATATTAATACA*	
sc1.18	F-AATTAACTTGACTTAATT	ns[b]
sc1.22	F-AAAATTAACTTGACTTAATTTT	29.3 ± 5.5
sc1.24	F-CAAAATTAACTTGACTTAATTTTG	6.1 ± 1.3
sc2.18	F-TGTTAAGGTATATTAATA	ns[b]
sc2.24	F-CTATGTTAAGGTATATTAATACAG	45 ± 6
sc.51	F-GGCAAAATTAACTTGACTTAATTTTTATGTTAAGGTATATTAATACAGTGG	2[c]

[a]Unlabeled complementary DNA strands were used to create labeled duplexes. Site I in the *scaC* promoter is in bold, and site II is in italics. Inverted repeats are underlined in each sequence where they are intact. [b]Nonspecific binding. [c]Not a dissociation constant but represents the concentration of free ScaR giving 50% DNA binding.

DNA-Binding Assays. The stoichiometry and affinity of ScaR−DNA binding were measured using fluorescence anisotropy-based assays. Dilute solutions of ScaR were titrated into solutions of fluorescein-labeled duplex DNA (Oligos Etc., Wilsonville, OR) in the presence or absence of an activating metal ion, and anisotropy measurements were made using a PanVera Beacon 2000 fluorescence polarization system. Oligonucleotide duplexes used in these studies are listed in Table 1. The sequences of these duplexes are related to the *scaC* operator, which has previously been described as possessing two ScaR recognition sequences, labeled I and II (*7*). The duplexes were prepared as described previously (*16*) in 25 mM HEPES, pH 7.

DNA-binding stoichiometry was determined for the interaction of ScaR with both sc1.22 and sc.51 (Table 1). For the 51 base pair oligomer, the reaction was performed in binding buffer (25 mM HEPES, 7.5, 500 mM NaCl, 10% glycerol) at 25 °C containing 50 nM duplex DNA and 1 mM $MnCl_2$. Under these conditions, the ScaR dimer was found to bind in a 2:1 stoichiometry with the 51 base pair stretch of DNA. However, for the 22 base pair fragment of DNA, a lower concentration of sodium chloride was used (50 mM) to increase the affinity of ScaR for the DNA duplex, and a slightly lower concentration of sc1.22 was used as well (25 nM).

The affinity of ScaR for various duplex DNA fragments was measured by titrating 1−10 μM solutions of ScaR dimer into 1 mL of binding buffer containing 1 mM $MnCl_2$. Titrations were performed at 25 °C, and measurements were made following a 60 s incubation period to allow equilibration. Where 1:1 binding stoichiometry between ScaR and the duplex was expected, data were fit to either eq 1 or eq 2. Equation 1 describes a simple 1:1 interaction between the protein dimer and the DNA duplex, where the DNA concentration is at least 10-fold below the measured dissociation constant. When the dissociation constant was observed to be less than 10-fold in excess of the concentration of DNA, eq 2 was used for curve fitting.

$$r = (r_{max} - r_{min})\left(\frac{P}{K_d + P}\right) + r_{min} \quad (1)$$

$$r = (r_{max} - r_{min})\left(\frac{K_d + D + P - \sqrt{(K_d + D + P)^2 - 4DP}}{2D}\right) + r_{min} \quad (2)$$

In eqs 1 and 2, r is the measured anisotropy, while r_{min} and r_{max} are the anisotropies of unbound and fully bound DNA, respectively. P is the concentration of ScaR, D is the concentration of fluoresceinated DNA, and K_d is the dissociation constant of ScaR from the oligonucleotide (*19*). Titrations of sc.51 were repeated in binding buffer supplemented with 50 mM $MgCl_2$ in order to lower the affinity of ScaR for the target DNA sequence, which permitted analysis of the data using the Hill equation (eq 3), in which n is the Hill coefficient and K_{50} is the concentration of ScaR that gives 50% maximal binding.

$$r = (r_{max} - r_{min})\left(\frac{P^n}{(K_{50})^n + P^n}\right) + r_{min} \quad (3)$$

The ability of various metal ions to activate ScaR for DNA binding was performed using fluorescence polarization assays as described above. In these studies, sc1.22 was used as the target duplex DNA due to the more moderate affinity of ScaR for this fragment relative to the longer sc1.24 fragment, permitting more general application of eq 1 in curve fitting. The assays were performed as above, except that the chloride salts of Mn^{2+}, Co^{2+}, Ni^{2+}, Zn^{2+}, and Cd^{2+} were used in concentrations ranging from 1 μM to 1 mM. The addition of zinc failed to activate ScaR for DNA binding.

Metal-Binding Stoichiometry and Affinity. The stoichiometry of Mn^{2+} binding to ScaR was investigated by neutron activation analysis and atomic absorption spectroscopy. For atomic absorption analysis, a solution of 100 μM ScaR incubated with 1 mM $MnCl_2$ in Na buffer was used (25 mM HEPES, pH 7.5, 200 mM sodium chloride, and 10% glycerol). For neutron activation analysis, NoNa buffer (25 mM HEPES, pH 7.5, 200 mM ammonium acetate, and 10% glycerol) was used to reduce background from activated sodium. The mixture of ScaR and Mn^{2+} was incubated at room temperature for 30 min prior to the separation of free Mn^{2+} from the ScaR·Mn^{2+} complex using Pierce spin desalting columns preequilibrated in the appropriate buffer. The concentration of ScaR in the eluate was determined by UV spectroscopy. Galbraith Analytical Laboratories (Knoxville, TN) performed the atomic absorption analysis. Neutron activation analysis was performed on samples and standards at the Reed College research reactor facility. Following irradiation at an average flux of 1.7×10^{12} neutrons/cm^2, gamma spectroscopy was performed at 1811 keV to measure decay from ^{56}Mn ($t_{1/2}$ = 2.58 h) formed during the irradiation. Background controls were performed in which ScaR was omitted from the samples applied to the spin column. The amount of free manganese detected from these controls

was subtracted from that obtained with the ScaR-containing samples.

Metal ion titrations of ScaR were performed by isothermal titration calorimetry (Microcal). A concentrated sample of ScaR (100 μM) was titrated with 2.5 mM $MnCl_2$ or 2.5 mM $CdCl_2$ in buffer B. The effect of pH on metal binding was investigated by performing similar titrations at pH 6.0 (25 mM Bis-Tris, pH 6.0, 200 mM NaCl, 10% glycerol). Data were fit to a variety of models for single and multiple site binding provided with the curve-fitting software, Origin 7.0 (OriginLab).

In addition, an assay that couples metal ion binding to DNA binding was developed. At sufficiently high concentrations of sc1.22 in low salt buffer (25 mM HEPES, 7.5, 50 mM NaCl, 10% glycerol), activated ScaR binds to the DNA duplex stoichiometrically, while apo-ScaR does not bind at all. Thus, the concentration of activated ScaR can be measured by fluorescence polarization so long as its concentration does not exceed the concentration of the target DNA sequence. Working in 1 mL solutions containing 50−100 nM sc1.22 and 25−50 nM ScaR dimer, a concentrated stock of $MnCl_2$ was added in small aliquots until the final concentration of manganese exceeded 3 μM. Following each addition, the anisotropy of the solution was measured. Data were fit to eq 2 as the measured dissociation constants were less than 10-fold greater than the concentration of ScaR subunits used in the titrations.

Size Exclusion Chromatography. The oligomeric state of ScaR with and without Mn^{2+} was determined using size exclusion chromatography. A Superdex 20/60 200 column (Amersham Pharmacia Biotech) was loaded with 2.8 mL of 3 mg/mL ScaR and eluted in 25 mM HEPES, pH 7.5, 200 mM NaCl, and 10% glycerol in either the presence or absence 1 mM $MnCl_2$. The elution profile was used to determine size from a standard curve as previously described (*20*). Briefly, the void volume of the column was determined with blue dextran, and calibration was performed with ribonuclease A (13.7 kDa), carbonic anhydrase (29 kDa), bovine serum albumin (66 kDa), and alcohol dehydrogenase (150 kDa). $K_{average}$ was calculated from eq 4.

$$K_{average} = \frac{V_E - V_O}{V_T - V_O} \quad (4)$$

where V_T, V_E, and V_O are the total volume, volume of elution, and void volume, respectively. $K_{average}$ was plotted vs the logarithm of molecular mass, and the resulting linear relationship was used to determine the molecular mass of ScaR.

Analytical Sedimentation Equilibrium Ultracentrifugation. The oligomeric state of ScaR in solution was determined using analytical ultracentrifugation. Experiments were performed on a Beckman XL-1 analytical centrifuge in the Biophysics Instrumentation Facility at UCSD. Experiments were performed at 35000 rpm and 25 °C using an An-60 Ti rotor with a path length of 1.2 cm. ScaR concentration was held at 25 μM in buffer B, and runs were performed with apo-ScaR absent any additives and in the presence of 100 μM EDTA, 1 mM $CoCl_2$, or 1 mM $CdCl_2$. To obtain the apparent molecular mass, the data were fit to eq 5:

$$A_r = A_o \exp[HM(r^2 - r_o^2)] + E \quad (5)$$

where

$$H = (1 - v\rho)\omega^2/2RT \quad (6)$$

and where A_r is the absorbance at radius r, A_o is the absorbance at the reference radius r_o, M is the molecular mass, E is the baseline offset, v is the partial specific volume of ScaR (0.7945 mL/g calculated using Sednterp), ρ is the solvent density (1.035 g/mL), and ω is the angular velocity.

Crystallization. Solutions of ScaR (25 mg/mL) were diluted with an appropriate volume of a 1 mM solution of duplex DNA containing the 22 base pair *scaC1* operator sequence and overhanging T bases at the 5′ end of each strand (5′-TAAAATTAACTCGAGTTAATTTT) and a stock solution of $MnCl_2$ such that the final solution contained 250 μM ScaR dimer, 350 μM duplex DNA, and 5 mM Mn^{2+}. Similar solutions were prepared with 1 mM $CdCl_2$ and 1.5 mM $ZnCl_2$. Crystals were grown using the hanging drop vapor diffusion method by mixing equal volumes of the ScaR·DNA·metal^{2+} solution and a well solution containing 1.6 M Li_2SO_4 and 0.05 M sodium cacodylate, pH 6.0. Following incubation of the crystallization setup at room temperature, large, rod-shaped crystals grew over 2 weeks to a maximum dimension of 1 mm in length and 0.2 mm in depth and breadth. Prior to data collection, crystals were transferred to a solution containing 1.8 M Li_2SO_4, 0.05 M sodium cacodylate, pH 6.0, and 10% (v/v) glycerol and flash-cooled by scooping the crystal from the cryoprotectant solution and plunging it into liquid nitrogen. Molecular replacement was unsuccessful, using either DtxR or IdeR as search models, so heavy atom methods of structure solution were pursued. A selenomethionine derivative of ScaR was prepared using standard methods (*21*) and was purified and crystallized in a similar fashion. A thimerosal (ethylmercuric thiosalicylate) derivative of ScaR was prepared from crystals grown in the presence of Mn^{2+}. Crystals were placed in a solution of 1 mM thimerosal in 1.8 M Li_2SO_4, 10% glycerol, and 0.05 M sodium cacodylate, pH 6.0, and incubated overnight. Data collection followed flash-cooling of the crystal as described above.

Data Processing and Structure Solution. Diffraction data were collected using an in-house system, which includes an R-Axis IV imaging plate detector coupled to a Rigaku RU300 rotating anode, or at synchrotron beamlines (Table 2) and were processed using Mosflm or D*trek (*22*, *23*). The original structure solution of apo-ScaR was determined using crystals grown in the presence of Mn^{2+}. A single heavy atom derivative, containing thimerosal, was used to obtain single isomorphous replacement solution. Initial phase determination was performed using Solve (*24*), followed by density modification and phase extension as implemented in CNS (*25*). Following initial model building, strict 2-fold noncrystallographic symmetry was used to improve maps. The resulting electron density map permitted construction of the majority of the ScaR dimer appearing in the asymmetric unit, but refinement of the model using CNS stalled with an *R*-factor above 0.35. Additional phase information was obtained by using single wavelength anomalous diffraction methods, as implemented in Solve, with a selenomethionine-containing derivative of ScaR crystallized in the presence of Mn^{2+}. Following phase combination, an improved map was obtained, and further refinement continued in CNS followed by TLS refinement as implemented in Refmac5 in the CCP4 suite or in Phenix (*26*−*28*) using TLS domains identified using TLSMD (*29*). Structures of the zinc and cadmium complexes of ScaR were solved by molecular replacement, and models were similarly refined in CNS, Refmac5, and PHENIX. The stereochemical quality of the models was determined using Procheck software (*30*). Helix angles were measured using Interhlx (K. Yap, University of Toronto).

Table 2: Crystallization and Refinement Statistics for Apo-ScaR and ScaR Bound to Cd^{2+} and Zn^{2+}

	apo-ScaR				
	derivatives				
	thimerasol (SIR)	SeMet (SAD)	native	ScaR·Cd^{2+}	ScaR·Zn^{2+}
data collection					
space group	$P4_12_12$	$P4_12_12$	$P4_12_12$	$P4_12_12$	$P4_12_12$
unit cell dimensions (Å)	a, b = 70.8; c = 301.8	a, b = 70.3; c = 301.8	a, b = 70.6; c = 301.5	a, b = 70.9; c = 304.1	a, b = 70.7; c = 301.9
X-ray source	Cu Kα	ALS 8.2.1	ALS 8.2.1	ALS 8.2.1	ALS 4.2.2
wavelength (Å)	1.5418	0.9795	1.0781	1.0781	1.2131
resolution range (Å)[a]	51.3−3.19 (3.37−3.19)	64.6−2.80 (2.95−2.80)	70.7−2.7 (2.85−2.70)	30.6−2.8 (2.91−2.80)	50.0−2.9 (3.00−2.90)
observations	57553	107601	148752	69627	108026
unique reflections	12581	18536	21544	18587	17514
completeness	94.0 (72.1)	94.9 (73.4)	97.5 (90.7)	92.9 (77.3)	96.9 (79.2)
$I/\sigma(I)$	9.1 (2.1)	8.3(2.1)	7.6 (2.4)	4.3 (2.4)	10.7 (2.0)
R_{merge} (%)[b]	6.4 (36.5)	5.5 (36.7)	6.8 (35.6)	8.4 (31.1)	7.1 (44.9)
phasing					
sites in asu[c]	3	5			
resolution range	20.0−3.5	20.0−3.2			
R_{deriv}	19.8				
phasing power	1.48				
figure of merit	0.33	0.30			
refinement					
resolution (Å)			20.0−2.7	20.0−2.8	20.0 − 2.9
R_{cryst}/R_{free} (%)[d]			22.3/27.2	23.0/28.2	23.1/29.2
no. of atoms					
protein			3447	3400	3344
solvent and solute			34	10	29
metal ions			0	2	2
rmsd bonds (Å)			0.008	0.008	0.010
rmsd angles (deg)			1.22	1.20	1.41
Ramachandran plot[e]					
most favored (%)			87.3	84.3	88.3
additionally allowed (%)			12.4	14.9	10.1
generously allowed (%)			0.3	0.5	1.6
disallowed (%)			0	0.3[f]	0
B factors (Å^2)					
protein atoms			108	127	107
metal ions				115	100
solute/solvent atoms			112	172	106

[a]Numbers in parentheses reflect the highest resolution shell. [b]$R_{merge} = \sum_h\sum_j|I_{h,j} - \langle I_h\rangle|/\sum_j\sum_h|I_{h,j}|$, where $I_{h,j}$ is the jth observation of reflection h. [c]Asymmetric unit. [d]$R_{cryst} = \sum_h||F_o| - |F_c||/\sum_h|F_o|$, where F_o and F_c are the observed and calculated structure factors for reflection h. R_{free} is calculated similarly for 10% of the data not used in refinement. [e]Determined using PROCHECK software (*31*). [f]One residue is in a disallowed conformation: Gln32 in the B chain.

RESULTS

Purification. The *scaR* gene is readily expressed in *E. coli* and typically yields 100−200 mg of apparently homogeneous, native ScaR protein from 2 L of culture following two chromatography steps. The protein may be stored at −80 °C indefinitely, retaining its activity as well as its ability to form crystals. Amino acid analysis (AAA Service Laboratory, Boring, OR) confirmed the identity of the protein product and was used to obtain a molar absorptivity of 18600 M^{-1} cm^{-1} for purified ScaR (based on subunits).

DNA-Binding Stoichiometry and Specificity. Previous analysis of the *scaC* operator region suggested that there are two ScaR binding sites associated within a 44 base pair region protected by ScaR in a DNA-footprinting study (Table 1 (*7*)). The first putative ScaR binding site, identified as site I, is composed of inverted repeats of an eight base pair sequence separated by six base pairs, while the second putative site (site II) was predicted to consist of an inverted repeat of a nine base pair sequence with no intervening base pairs (*7*). To test ScaR binding to these sites, DNA-binding studies were performed with a series of fluorescently labeled DNA duplexes containing portions of the *scaC* operator sequence in the presence of 1 mM Mn^{2+} (Table 1).

The stoichiometry of ScaR−DNA interactions supports the previous analysis. When duplex DNA containing the full 46 base pair sequence, sc.51, is used, it is observed that ScaR saturates the DNA when there are 2.0 ± 0.1 (n = 4) dimers per DNA fragment, while a smaller fragment of DNA containing a 22-bp sequence derived from site I binds to ScaR in a 1.0 ± 0.1 (n = 3) molar ratio (Figure 2).

The extent of sites I and II, and the potential interaction of ScaR dimers bound at each site, was evaluated by comparing the affinity of the protein for 18-bp duplexes vs 24-bp duplexes and to sc.51, which contains the full *scaC* operator sequence. Weak nonspecific binding was observed with 18-bp duplexes (sc1.18 and sc2.18; Table 1), but high-affinity interactions take place between ScaR and 24-bp fragments. The ScaR·Mn^{2+} complex binds sc1.24 with a K_d of 6.1 ± 1.3 nM, roughly an order of magnitude more tightly than sc2.24, which binds with a K_d of 45 ± 6 nM (Figure 3). These results indicate a preference for a larger region associated with site II than previously described (*7*) and have led to the conclusion that both sites are composed of

8-bp inverted repeats separated by six base pairs, giving a recognition sequence that extends over 22 bp at each site. Also, ScaR apparently possesses a greater affinity for the symmetric site I. Comparison of the these dissociation constants to the affinity of ScaR for the sc.51 duplex reveals slightly tighter binding to the latter. The concentration of free ScaR·Mn^{2+} complex that gives apparent 50% binding to sc.51, 2 nM, is lower than the dissociation constant of ScaR·Mn^{2+} from sc1.24. Quantification of the equilibrium interactions between two dimers of the ScaR·Mn^{2+} complex and 1 nM sc.51 is rendered algebraically complex by the relatively tight binding at 500 mM NaCl, which requires an adjustment for the loss of free protein concentration in the assays, as in eq 2. Therefore, we also examined the ScaR·Mn^{2+}·sc.51 interaction in the presence of 50 mM $MgCl_2$, which reduces the affinity of ScaR for DNA, presumably through electrostatic screening (Figure 3B). Application of the Hill equation yields a coefficient of 1.72 ± 0.14 (with the concentration of ScaR dimer giving 50% binding at 14.7 ± 0.8 nM). These results further support the presence of significant cooperativity in binding between ScaR dimers to the full-length operator sequence (Figure 3).

Metal-Dependent Activation of ScaR for DNA Binding. The ability of various metal ions to activate ScaR for DNA binding was investigated using the fluorescence anisotropy assay with sc1.22 as the target DNA sequence. The shorter sequence was used to avoid the tight binding that complicated curve fitting when sc1.24 was used. Five divalent metal cations were assayed: Mn^{2+}, Co^{2+}, Ni^{2+}, Zn^{2+}, and Cd^{2+}. Only Zn^{2+} failed to promote strong DNA binding under the conditions of our assay, even when added to a concentration of 1 mM. For the activating metals, the total change in anisotropy achieved at saturation was relatively constant between metals, typically varying from 0.018 to 0.025, from a starting anisotropy of between 0.065 and 0.070. The ability of each metal to activate ScaR was determined over a range of metal ion concentrations (Table 3). Cadmium is clearly the strongest activating metal ion of the three and activates ScaR 10-fold better at 1 mM concentration than manganese, cobalt, or nickel (Figure 4). At 1 μM cadmium, specific binding of ScaR to sc1.22 is still observed, while neither manganese or cobalt is capable of achieving significant activation of ScaR at a similar concentration. Interestingly, the affinity of ScaR for its cognate DNA sequence is nearly maximized at 100 μM Cd^{2+} but can be enhanced by increasing the concentration of Mn^{2+} from 100 μM to 1 mM (Table 3), indicating weaker affinity for manganese. Moreover, cadmium permits tighter binding of ScaR to sc1.22 than any other metal tested.

Metal Binding to ScaR. Both atomic absorption spectroscopy and neutron activation analysis reveal multiple Mn^{2+} ions

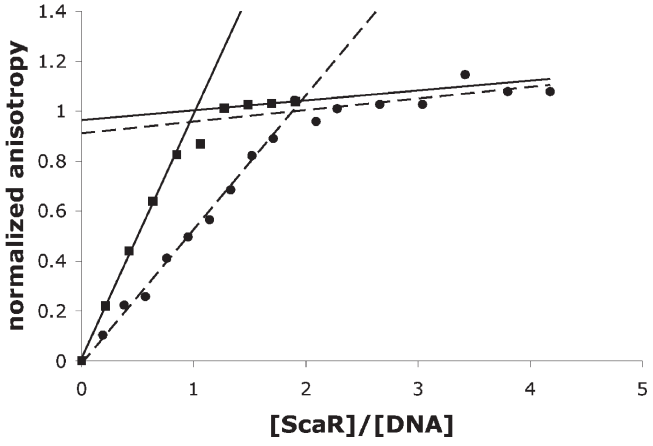

FIGURE 2: Stoichiometry determination for binding of ScaR to duplex DNA. (●) ScaR·Mn^{2+} binding to sc.51. (■) ScaR·Mn^{2+} binding to sc1.22. Lines are fit separately to data preceding and following the stoichiometric equivalence points.

Table 3: Dissociation Constant of ScaR Dimers from sc1.22 in the Presence of Different Activating Metals[a]

	K_d (nM) at the given concn of metal ion				
metal ion	1 μM	10 μM	100 μM	1 mM	change in anisotropy[b]
Mn^{2+}	ns	960 ± 160	210 ± 13	29.3 ± 5.5	0.024
Cd^{2+}	54 ± 21	15 ± 6	5.8 ± 2.2	2.3 ± 0.1	0.024
Co^{2+}	nd	ns	245 ± 17	28.0 ± 2.6	0.025
Ni^{2+}	nd	nd	47 ± 12	22.4 ± 6.4	0.018
Zn^{2+}	nd	ns	ns	ns	

[a]ns indicates nonspecific, low-affinity interactions between ScaR and the DNA duplex, and nd indicates that no measurement was made. All dissociation constants are the average of three trials. [b]Total change in anisotropy observed 1 mM metal ion concentration. These values represent increases of 27−37% relative to the initial anisotropy.

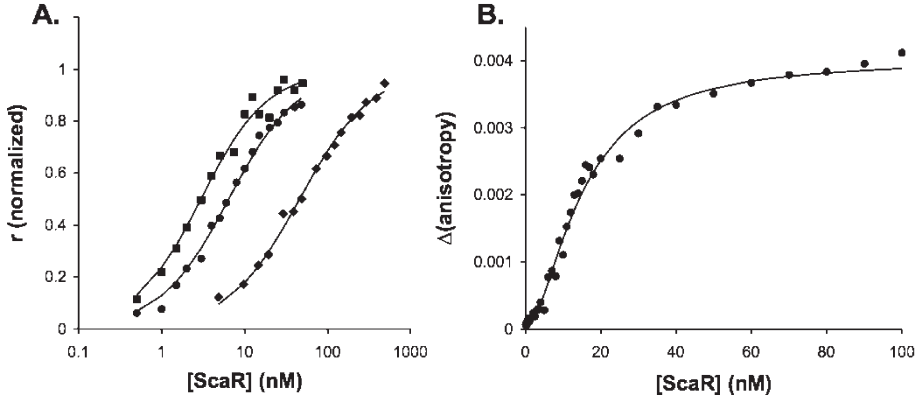

FIGURE 3: (A) Binding isotherms for ScaR and duplex DNA containing operator sequences obtained from fluorescence anisotropy assays performed in binding buffer (25 mM HEPES, pH 7.5, 500 mM NaCl, 10% glycerol) with the horizontal axis presented logarithmically. Key: (■) ScaR·Mn^{2+} binding to sc.51, (●) ScaR·Mn^{2+} binding to sc1.24, and (◆) Scar·Mn^{2+} binding to sc2.24. Curve fits assume 1:1 binding stoichiometry between ScaR and the DNA duplex, though ScaR binds in a 2:1 stoichiometry to sc.51. (B) Binding isotherm of ScaR with sc1.51 performed in binding buffer supplemented with 50 mM $MgCl_2$. The data presented are the average of three trials. The curve is derived from a fit of the Hill equation, with a Hill coefficient of 1.72 ± 0.14.

binding per ScaR subunit. In two replicates, the Mn^{2+}:ScaR ratio was found to be 2.6 ± 0.4 by atomic absorption spectroscopy. Three replicates performed using neutron activation analysis yielded a value of 2.8 ± 0.3 for the ratio of Mn^{2+} bound to ScaR at pH 7.5.

Calorimetric titrations of ScaR with Mn^{2+} likewise support multiple Mn^{2+}-binding sites per subunit. When titrating Mn^{2+} into a solution of ScaR at pH 8, a biphasic thermal signature is observed, in which the first metal binds endothermically with an association constant of (4.5 ± 1.3) × 10^4 M^{-1} and the second binds exothermically with an association constant of (1.3 ± 0.5) × 10^5 M^{-1} (Figure 5), values corresponding to dissociation constants of 22 ± 6 μM and 8 ± 4 μM, respectively. To achieve a satisfactory curve fit, the concentration of ScaR was assumed to be 85% of that calculated by UV absorbance. Use of a three-site sequential model did not improve the fit. Efforts to perform calorimetric titrations of ScaR with Cd^{2+} yielded curves

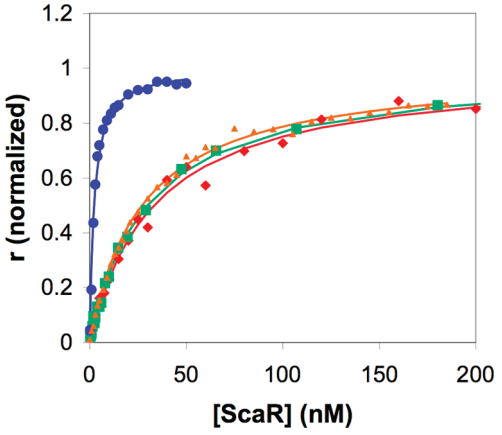

FIGURE 4: Assay of metal ion activation of ScaR using fluorescence anisotropy. The assays were performed with 1 nM sc1.22 in buffer B containing 1 mM of the following metals: Cd^{2+} (blue circles), Co^{2+} (orange triangles), Ni^{2+} (green squares), and Mn^{2+} (red diamonds). The data were fit to binding equations assuming 1:1 stoichiometry between the ScaR dimer and the target DNA duplex.

that could not readily be modeled (Figure 5C) but likewise indicate a stoichiometry of multiple metal ions per subunit, and titrations with zinc resulted in significant problems with baseline variation in the titrations (data not shown). These difficulties may be the result of an aggregation phenomenon that we commonly observed with relatively concentrated (>10 μM) solutions of ScaR in the presence of cadmium and zinc (see below).

To obtain information on the effect of pH on Mn^{2+} binding, ITC was also performed at pH 6 with $MnCl_2$ as a titrant. A weak endothermic signal was obtained that did not saturate with a 5-fold molar ratio of Mn^{2+} to ScaR. Modeling the binding with 1:1 binding stoichiometry yielded a satisfactory fit with a dissociation constant of 0.5 ± 0.1 mM and a binding enthalpy of 3.5 ± 0.5 kcal/mol (Figure 5B). Given the weak signal, these results must be viewed as provisional, but clearly the affinity of manganese for ScaR is diminished at lower pH.

In a separate assay of manganese binding to ScaR, metal binding was coupled to DNA binding in a fluorescence anisotropy-based assay. This assay is distinct from the one used to measure the dissociation of ScaR from duplex DNA in that constant and near stoichiometric concentrations of both ScaR and duplex DNA were present throughout the titration with Mn^{2+}. Working at high DNA concentrations (>50 nM) promotes stoichiometric binding with ScaR·Mn^{2+}. Rigorously demetalated solutions were used in these titrations, and no binding of protein to DNA was observed in the absence of added metal. The plots of anisotropy vs manganese concentration could be satisfactorily fit to a binding model assuming a 1:1 stoichiometry of metal binding to each subunit of ScaR (Figure 6), yielding a dissociation constant of 0.24 ± 0.07 μM. This value is roughly 100-fold lower than the dissociation constants measured by ITC and is certainly much lower than the concentrations of manganese required to activate ScaR in the DNA-binding trials (Table 3). The affinity of ScaR for manganese is likely heightened due to linkage of metal binding with a thermodynamically favorable DNA-binding event in this assay. The 1:1 stoichiometry assumed in obtaining the curve fit indicates that a single

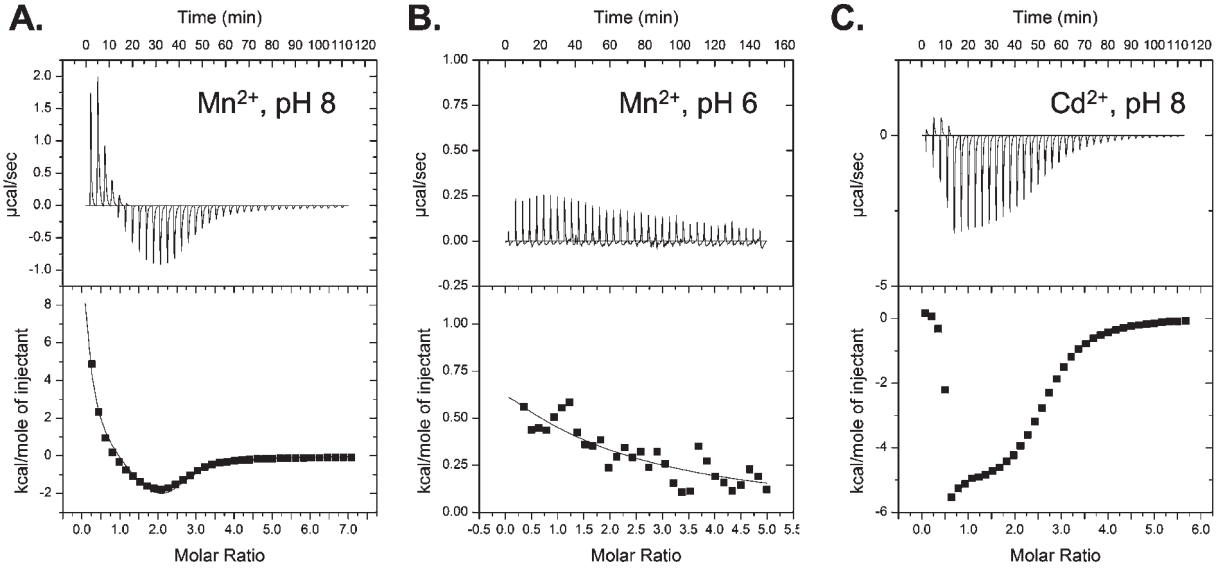

FIGURE 5: Results of isothermal titration calorimetry. (A) Titration of 2.5 mM $MnCl_2$ into a solution of 100 μM ScaR (measured as subunits by UV spectroscopy) at pH 8. The curve reflects a fit of the data to a sequential two-site binding model: K_{a1} = (3.6 ± 1.7) × 10^4 M^{-1}, $\triangle H_{d1}$ = 16 ± 6 kcal/mol, K_{a2} = (1.8 ± 0.9) × 10^5 M^{-1}, $\triangle H_2$ = −18 ± 6 kcal/mol. The apparent concentration of ScaR is 85 μM. (B) Titration of 2.5 mM $MnCl_2$ into a solution of 100 μM ScaR at pH 6. The curve reflects a 1:1 binding model of Mn^{2+} to ScaR: K_a = (2.1 ± 0.5) × 10^3 M^{-1}, $\triangle H$ = 3.6 ± 0.5 kcal/mol. (C) Titration of 1 mM $CdCl_2$ into 100 μM ScaR.

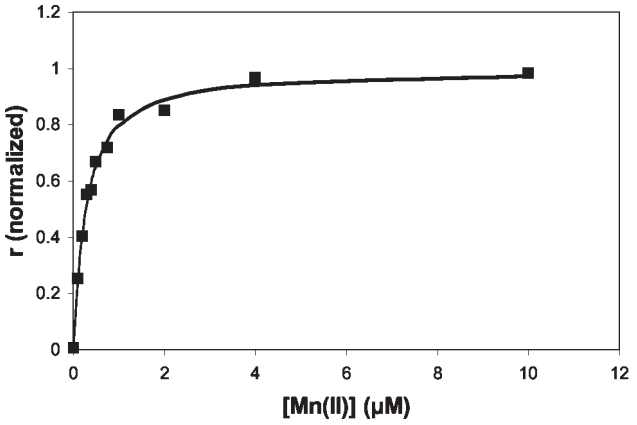

FIGURE 6: Binding isotherm obtained from fluorescence anisotropy-based assay for manganese binding by ScaR. Assuming a 1:1 stoichiometry for Mn^{2+} binding to ScaR subunits, a dissociation constant of 240 ± 70 nM is obtained.

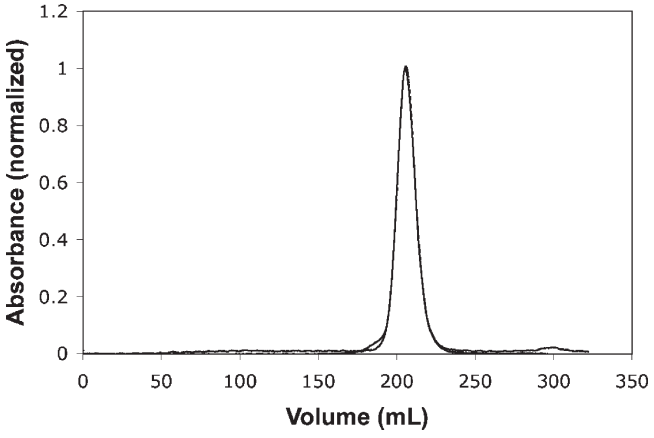

FIGURE 7: Size exclusion chromatography analysis of ScaR monitored by absorbance at 280 nm. The elution was performed in the presence (black line) and absence (gray line) of 1 mM $MnCl_2$.

metal-binding event per subunit is necessary to activate ScaR with Mn^{2+}. Likewise, it suggests that the activating sites on the individual subunits are independent of each other.

Oligomeric State of ScaR in Solution. Size exclusion chromatography was used to determine the oligomeric state of ScaR in solution in the presence and absence of 1 mM Mn^{2+}. The elution profiles of the protein sample under both conditions are quite similar (Figure 7) and lead to calculated molecular masses of 57.8 and 56.6 kDa for the samples with and without Mn^{2+}, respectively. Given a calculated molecular mass of 24.8 kDa per subunit, these results suggest that ScaR retains a dimeric state in both the presence and absence of manganese.

To confirm the dimeric state of apo-ScaR, analytical ultracentrifugation was performed. Sedimentation equilibrium measurements using 25 μM solutions of apo-ScaR (measured as the monomer) can be fit to a single species with an apparent molecular mass of 45400 ± 400 Da (Figure 8). This compares well to the predicted dimeric mass of 49.5 kDa for ScaR. The addition of 100 μM EDTA does not appreciably affect that result. In solutions of moderate ScaR concentration, such as those used in ITC, we expect that the bulk of the protein is in its dimeric state, even in the absence of activating metal ions, though it may be that more dilute solutions exist in a monomer−dimer equilibrium.

Structure of ScaR in the Crystalline State. Large tetragonal crystals of ScaR can be grown from concentrated lithium

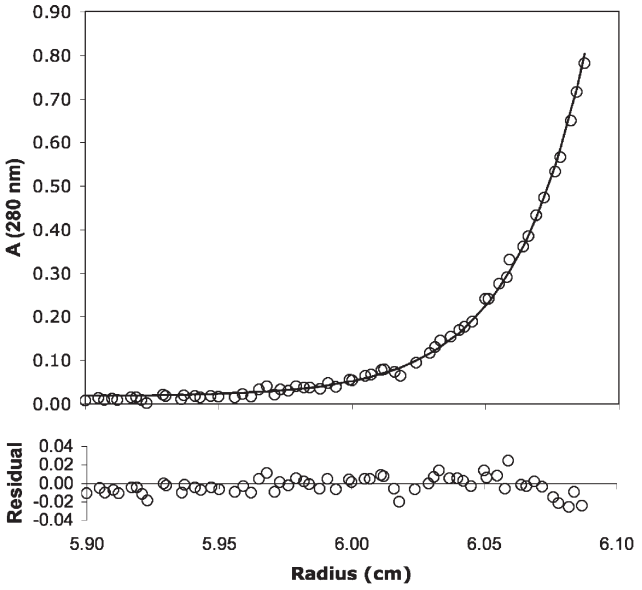

FIGURE 8: Analytical ultracentrifugation data obtained with apo-ScaR monitored by absorbance at 280 nm. Data were fit to eq 5 and yielded a molecular mass of 45400 ± 400 Da, indicating that apo-ScaR maintains a dimeric state in solution at 25 μM concentration.

sulfate solutions at pH 6.0 in the presence of a duplex DNA fragment containing the *scaC1* operator sequence and metal ions, including Mn^{2+}, Zn^{2+}, and Cd^{2+}. However, the crystals do not contain DNA, and in the case of crystals grown in the presence of manganese, no bound metal was observed in the structure either. In structures solved from crystals grown in the presence of cadmium and zinc, a single metal ion is observed bound to each ScaR subunit. Structure solution of apo-ScaR (grown from Mn^{2+}-containing solutions) proceeded in two stages, with initial model fitting to a map obtained by SIR methods using a thimerasol derivative of ScaR crystals (Table 2) and a native data set that extended to 3.0 Å. However, ambiguity in that map required further efforts at phase determination, which were facilitated by crystals of a selenomethionine-containing variant of ScaR and the use of SAD methods. Lastly, a native data set collected to 2.7 Å was used in the refinement of the final model of ScaR in its metal-free state. Subsequent crystals of ScaR bound to cadmium and zinc were isomorphous to the apo-ScaR crystals, and structures were obtained by molecular replacement. The asymmetric unit of these crystals contains a homodimer of ScaR, the presumed functional unit of the protein, and is largely complete, except for residues 2−5 at the N-terminus of the B subunit (amino acid analysis indicated that the N-terminal methionine residues are cleaved from the protein). The model was obtained with satisfactory refinement statistics and stereochemical parameters (Table 2).

Like its homologues, the iron-binding proteins DtxR and IdeR (*12*, *31*), ScaR may be divided into three domains: an N-terminal DNA-binding domain comprising residues 2−72, which contains a winged helix−turn−helix DNA-binding motif (Figure 9); a central dimerization domain comprising residues 73−140, which forms contacts with the dyad-related subunit; and a C-terminal domain bearing sequence similarity to the FeoA protein involved in iron uptake in several bacterial species (*32*). In keeping with recently proposed terminology (*8*) and classification within the Pfam database (*33*), we have labeled the C-terminal 75 residues of the ScaR FeoA domain. The DNA-binding domain consists of three α-helices (α1−α3) with α2 and α3 forming the

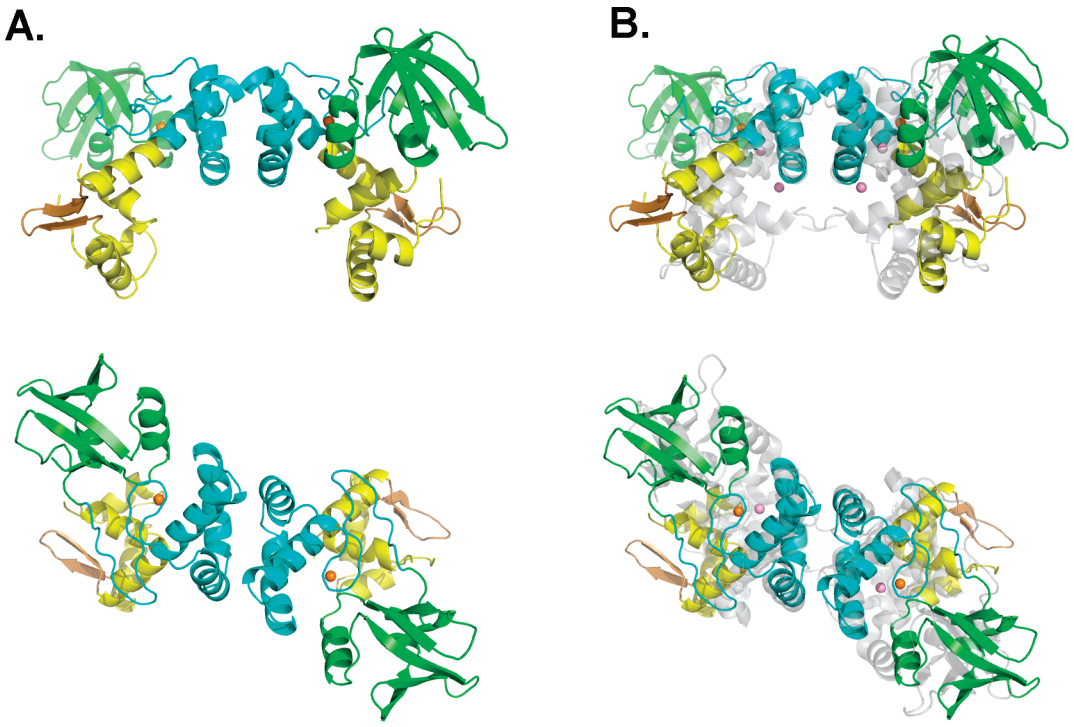

FIGURE 9: Structure of ScaR bound to Cd^{2+}. The coloring scheme for ScaR is as for IdeR in Figure 1. In addition, the wing in the DNA-binding domain is colored bronze. The cadmium ions are colored orange. (A) Two views, rotated by 90° about the horizontal axis. In the lower orientation, the DNA-binding domains are facing away from the viewer. (B) Identical views of ScaR (colored as in (A)) overlaid with IdeR, in gray at half-transparency. Co^{2+} ions bound to IdeR are shown in pink.

helix−turn−helix (HTH) motif, followed by a pair of antiparallel β-strands that form a "wing" following the HTH motif (Figure 9 (*34*)). A long linker helix, α4, connects the DNA-binding domain to the dimerization domain, which is formed by helices α5 through α7 followed by a second pair of antiparallel β-strands linked by a β-turn (residues 122−126) that contribute to metal ion binding (see below). The arrangement of secondary structure elements in the C-terminal FeoA domain bears similarity to its namesake, the ferrous ion transport protein (Figure 10; PDB ID 3E19) as well as to the src homology 3 domain, as has been noted in DtxR and IdeR (*12*, *31*), and contains a five-stranded antiparallel β-sheet and two additional α-helices. The dimerization and FeoA domains of ScaR are connected by a conformationally heterogeneous stretch of residues (132−150) that is 11 residues shorter than the peptide region connecting the comparable domains of DtxR and IdeR.

In a structural alignment of the two subunits, the 208 residues present in both models of chains A and B superimpose with an rmsd in C_α atom positions of 0.69 Å. However, the overlap between individual domains is generally closer. The dimerization domains overlap with an rmsd of 0.33 Å and the FeoA domains by 0.40 Å. There is a greater structural deviation between DNA-binding domains (the rmsd is 0.69 Å), chiefly due to differences in structure of the flexible loop and the N-terminus. Within the two subunits, there is some variation with respect to domain positioning, demonstrating some positional independence between domains. When the dimerization domains of the two subunits are superimposed, the FeoA domains vary in position by a maximum of 1.2 Å (measured at residue 197) and the DNA-binding domains vary by 2.6 Å (at residue 40). The mobility of the DNA-binding domain with respect to the dimerization domain is centered at residue 72 of α4 and requires just a slight unwinding of the helix at that position without loss of hydrogen bonds

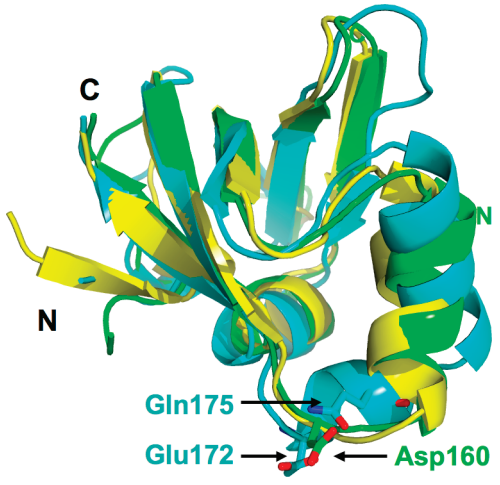

FIGURE 10: Structural alignment of the FeoA protein of *T. thioreducens* (PDB ID 3E19) in yellow with the C-terminal domains of ScaR (green) and IdeR (turquoise). The N- and C-termini of each are labeled, as are the side chains of metal-binding residue Asp160 from ScaR and Glu172 and Gln175 of IdeR.

within the helix. The presence of a bound metal ion does not significantly affect the tertiary structure of ScaR. An overlay of the cadmium complex of ScaR with the metal-free form shows a 0.53 Å rmsd between C_α atoms of the dimers.

The separation between the DNA-binding domains of the apo-ScaR dimer is larger than that observed in DtxR or MntR. When measured between the C_α atoms of Glu40, at the center of the recognition helix, the domain separation is 41 Å in ScaR, which is comparable to the largest value of 39 Å separation observed in one of the conformations of apo-MntR (*35*). The structure of apo-DtxR shows a separation of 28 Å between comparable positions (*36*). The heterogeneity of conformations observed

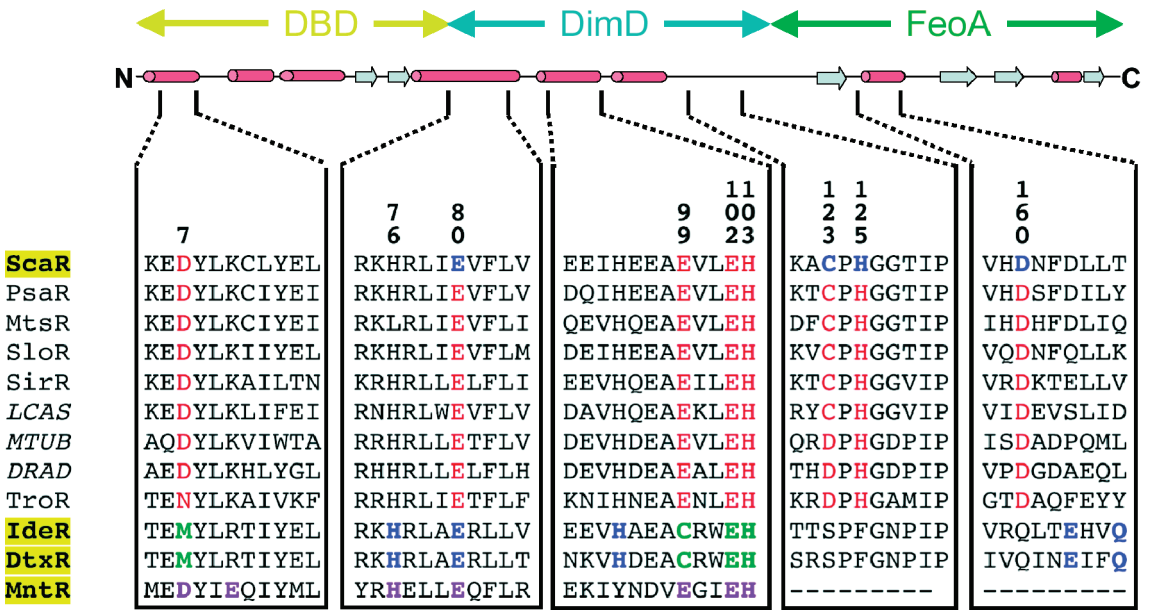

FIGURE 11: Sequence alignment of the metal-binding regions of ScaR with other members of the DtxR/MntR family of metalloregulators. Proteins for which structures exist are highlighted in yellow at the left. A secondary structure schematic above the alignment shows the relative positions of these regions in ScaR and their relationship to the DNA-binding domain (DBD), dimerization domain (DimD), and FeoA domain. Conserved residues that potentially play a role in metal binding are identified by residue number (ScaR numbering) above. Residues in blue have been observed to participate in metal binding in the secondary site (ScaR) or ancillary site (DtxR/IdeR). Residues in green have been observed participating in metal binding in the primary site (DtxR/IdeR). Metal-binding residues in MntR are given in purple. Residues colored red are predicted to bind metal ions based on analogy to existing crystallographic data, but no direct evidence exists for those roles as yet. ScaR, PsaR, MtsR, and SloR are streptococcal regulators. SirR is from *S. epidermitis*, LCAS is a metal regulator identified in the *Lactobacillus casei* genome (accessed at www.tigr.org), MTUB is a metal regulator identified in the *M. tuberculosis* genome (*37*), DRAD is a metal regulator identified in the *D. radiodurans* genome (*38*), and TroR is the Mn^{2+} regulator from *T. denticola* (*39*).

for apo-MntR suggests that crystal contacts may have a great deal to do with the observed separations between DNA-binding domains in the DtxR/MntR family. However, it is notable that the inverted repeats to which ScaR binds are separated by six base pairs, while the DtxR dimer binds operator sequences spanning 19 bp, with inverted repeats of nine base pairs separated by one base pair. The structure of ScaR generally favors greater separation of the DNA-binding domains, as the hinge helices (α4) in the ScaR dimer depart from each other at an angle of 110° vs an angle of 88° in apo-DtxR (this angle does not vary significantly in response to metal binding). As a result, the C_α atoms of His76 (a residue on helix 4 that is not affected by the hinge motion) are separated by 23.9 Å in the ScaR dimer but only by 19.7 Å in the DtxR dimer (*12*).

Metal-Binding Interactions. Based on sequence alignments, it was expected that at least one metal site in DtxR would be conserved in ScaR. The primary site, formed by Met10, Cys102, Glu105, and His106 in DtxR, is known to be essential for DNA binding (*13*). In ScaR, the analogous residues are Asp7, Glu99, Glu102, and His103 (Figure 11). No metal binding is observed to that site in any of the structures reported here, though the residues are positioned appropriately to form a binding site. The reason for the lack of bound metal at this putative site is unclear. Perhaps it is due to the low pH of crystallization, the high concentration (~3.2 M) of Li^+ ions competing for anionic sites, or some other factor of the crystallization process. While it must be considered possible that this site is not involved in metal binding in ScaR, that is unlikely given the broad conservation of metal-binding residues at appropriate positions, the functional importance of residues at comparable positions in DtxR as well as MntR, and the evidence for multiple metal-binding sites from solution studies reported here.

Despite the absence of structural evidence for metal binding to the primary site, metal binding is observed elsewhere in the protein. In the presence of Zn^{2+} and Cd^{2+} under crystallization conditions, ScaR binds one metal ion per subunit at a site composed of four residues: Glu80, from linker helix α4, Cys123 and His125 from a β-turn that acts as a metal-binding "flap", and Asp160 from the FeoA domain (Figure 12). This site is novel within the DtxR/MntR family. Only Glu80 aligns with another metal-binding residue in DtxR (Glu83; Figure 11). The other three residues are at positions that have not previously been assigned to a metal-binding function. We have labeled this site "secondary" to distinguish it from the "ancillary" site described in DtxR and IdeR, which is also composed of residues from the dimerization and C-terminal domains. The moderate resolution of the structures of ScaR presented here does not permit a detailed description of metal-binding geometry, but it appears that there is space for one or two additional water ligands, creating a pentavalent or hexavalent site. When the structures of ScaR and DtxR are superimposed by the positions of α carbons in the dimerization domain (residues 72−125; Figure 12), the secondary site in ScaR is roughly 5 Å distant from the position of the ancillary site in DtxR. Interestingly, two histidine residues (His76 and His95) in ScaR align with metal-binding residues His79 and His98 of DtxR, but neither of the ScaR residues appears to be positioned appropriately to bind metal. However, His76 is positioned so as to interact with Asp160, in the secondary site, and Glu102, a likely contributor to the putative primary site (Figure 12). Thus His76 may play a role in interactions between the two metal-binding sites of ScaR.

Sequence alignment of ScaR with a variety of DtxR family members reveals that the residues of the secondary binding site are highly conserved among related proteins found in

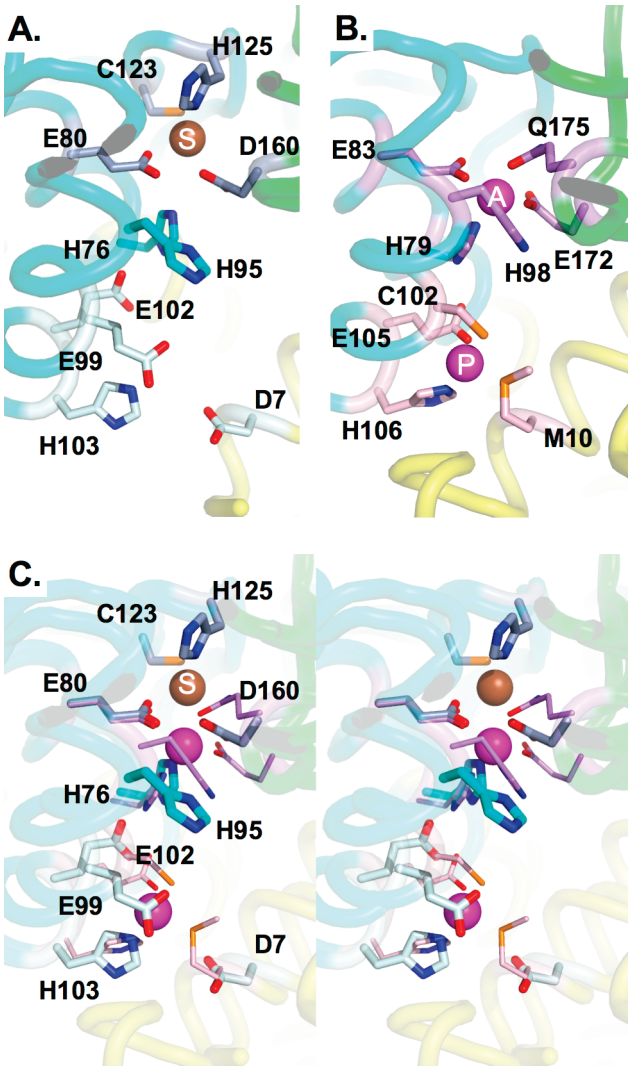

FIGURE 12: Metal-binding regions of ScaR and IdeR compared. (A) ScaR·Cd^{2+} complex. The coloring of the backbone is as in Figure 1. Residues observed to bind the secondary site metal have carbon atoms colored blue-gray, while the carbon atoms of putative primary site residues are colored light blue. Conserved residues His76 and His95 lie outside the occupied secondary site, but His76 is H-bonding to Asp160 and Glu102. (B) IdeR·Co^{2+} complex. The primary site metal is labeled "P", and the ancillary site metal is labeled with an "A". Carbon atoms of residues participating in each site are colored purple and pink, respectively. The coloring of the backbone is as in "A". (C) Stereoimage of the superposition of the ScaR·Cd^{2+} and IdeR·Co^{2+} complexes. The secondary site of ScaR is roughly 5 Å away from the ancillary site of IdeR.

streptococcal species. Furthermore, ligating residues are more generally found at positions associated with the secondary site of ScaR than with the ancillary site of DtxR among family members from a broad selection of microbial sources (Figure 11). Histidine 125 from the metal-binding flap is widely conserved, though it is replaced with a phenylalanyl residue at the comparable position in DtxR (Phe128). Cysteine 123, also in the flap, is likewise broadly conserved, but an aspartyl residue is often found in the analogous position as in TroR and the DtxR family regulator found in *Deinococcus radiodurans* (*38*, *39*). Interestingly, *M. tuberculosis* has two DtxR family member regulators, one of which (IdeR) is a close homologue of DtxR possessing an ancillary metal-binding site (*31*) and a second that is more similar to ScaR, having the residues necessary to create the secondary metal site (Figure 11).

DISCUSSION

We have investigated the structure and function of ScaR, the metalloregulatory protein responsible for manganese homeostasis in *S. gordonii*. The DNA-binding specificity of ScaR reflects affinity for sequences that are composed of an inverted repeat of the apparent consensus sequence 5′-AATTAAAA, separated by six intervening base pairs. The native *scaC* operator is constructed from two sites (I and II) possessing this sequence, and the ScaR dimer binds to short DNA fragments containing each sequence in 1:1 stoichiometry, albeit with higher affinity for the more symmetric site I. Likewise, two ScaR dimers bind to the full 46-bp *scaC* sequence with high affinity and positive cooperativity.

In order to bind its cognate DNA sequence, ScaR requires metal-ion activation. The results presented here indicate that ScaR is activated by a variety of different metal ions, including Mn^{2+}, Co^{2+}, Ni^{2+}, and Cd^{2+}, though Zn^{2+} does not promote DNA binding under the conditions of our assay. Cadmium is the strongest activator of ScaR, while Mn^{2+}, Co^{2+}, and Ni^{2+} activate ScaR similarly at a given concentration. These results are somewhat different than those presented by Jakubovics et al. (*7*), which showed greater relative specificity for Mn^{2+} over other metal ions and identified zinc and nickel as moderate activators. The earlier results were obtained under nonequilibrium conditions using a gel shift assay and were performed with a considerably longer fragment of duplex DNA than that used here (226 vs 22 bp). It may also be that Zn^{2+} interactions with DNA are influencing the binding assays. Zinc forms relatively strong interactions with the phosphate backbone (*40*) and also can influence DNA conformation (*41*). Nevertheless, there may be a physiological basis for the observed inability of zinc to activate ScaR. A recent report indicates that zinc can relieve manganese-mediated repression by PsaR, a close streptococcal homologue (*42*). In general, though, ScaR shows the capacity to be activated by a variety of metal ions, much like DtxR (*43*, *44*). That result does not necessarily negate the observation that ScaR responds selectively to manganese *in vivo* (*7*). As noted in a recent review, metal ion specificity may by achieved by "affinity, allostery, or access" (*45*). In the case of ScaR, lack of access to competing metals in the cell may play a greater role in determining its specificity than enhanced affinity for its cognate metal ion, manganese.

The mechanism of activation of ScaR by metal ions remains unclear. A linked metal-binding assay that is monitored through the activation of ScaR for DNA binding indicates that a single Mn^{2+}-binding event per subunit is necessary to activate ScaR (Figure 6). In contrast, solution studies aimed at uncovering the stoichiometry of manganese binding to ScaR indicate that there are at least two sites per subunit competent to bind Mn^{2+}. Stoichiometries obtained using spin desalting columns show that between 2 and 3 Mn^{2+} ions bind per subunit when 100 μM ScaR is incubated with 1 mM $MnCl_2$. Isothermal titration calorimetry experiments likewise indicate multiple binding sites on ScaR for Mn^{2+} and Cd^{2+}, with saturation of these sites occurring at submillimolar concentrations of either metal and with micromolar dissociation constants for Mn^{2+}.

The structural results provide limited insight into metal binding to ScaR. Crystallization of ScaR takes place at pH 6. We have observed diminished metal ion affinity at that pH, which at least partially explains the absence of bound metal when ScaR is crystallized in the presence of 1 mM Mn^{2+}. Likewise, the presumed primary site, which includes residues Asp7, Glu99,

Glu102, and His103, remains vacant when the protein is cocrystallized with cadmium and zinc. Again, part of the reason for the absence of bound metals at this site may be the low pH of the crystallization conditions. The high concentration of lithium sulfate (>1.6 M) may also play a role. In a related case, early structures of DtxR, determined using crystals grown from 2.0 M ammonium sulfate, often lacked bound metal at the primary site, and sulfate competed with protein ligands at the ancillary site (*46*). Clearly, it would be valuable to have direct evidence for metal binding to the primary site, and future experiments will investigate the role of residues presumed to participate in that site.

Nevertheless, the Cd^{2+}- and Zn^{2+}-containing structures do reveal a novel metal-binding site at the interface of the FeoA and dimerization domains. Distinct from either of the metal-binding sites in DtxR and IdeR, the secondary site of ScaR is comprised of residues Glu80, Cys123, His125, and Asp160. The functional importance of the secondary site remains unclear. Could the ancillary site of DtxR be used as a model? Although it is not essential for metal-dependent activation (*13*), the ancillary site has been implicated in both the stabilization of the active dimer and promoting the active arrangement of the C-terminal domain (*47*, *48*). In contrast to DtxR, ScaR is dimeric even in the absence of bound metal ions, and while the structure of ScaR is highly reminiscent of the structures of DtxR and IdeR (*12*, *18*, *31*), the relatively well defined position of the FeoA domain of ScaR is a significant structural difference, caused perhaps by the shorter linking polypeptide between the domains in ScaR. One of the presumed roles of the C-terminal domain in DtxR, the binding of a proline-containing polypeptide that spans the dimerization and C-terminal domains (*49*), is unlikely to be important in ScaR, since the shortened peptide lacks most of the proline residues found in the comparable peptide segment of DtxR.

Despite the absence of an obvious functional role associated with metal binding to the secondary site of ScaR, it is well-conserved among related proteins. A published phylogenetic tree including ScaR, some streptococcal homologues, SirR from *Staphylococcus epidermitis*, and TroR from *Treponema pallidum* indicates that these proteins form a distinct group within the DtxR/MntR family (*7*). This branch might be referred to as the Mn/Fe group, reflecting the mix of activities among these proteins, which is in contrast to the functional specificity associated with DtxR and MntR (*17*). The structural results presented here support the segregation of these proteins based on the conservation of the residues associated with the secondary site (Figure 11). While the primary site residues are generally conserved as metal-binding residues across the DtxR/MntR family (though the "primary" site is remodeled as the C site MntR), the secondary site is not. Instead, it may be replaced by the ancillary site of DtxR, the A site of MntR, or it may be altogether absent as appears to be the case in TroR from *T. pallidum* (*39*). In DtxR, the ancillary site is composed of His79, Glu83, His98, Glu172, and Gln175. Of those residues only the position related to Glu83 retains metal-binding function in ScaR (Glu80). The residues implicated in the secondary site by the work presented here (Glu80, Cys123, His125, and Asp160) are uniformly conserved as potential metal-binding residues in the Mn/Fe group. TroR from *T. pallidum* is the single exception, since it lacks the FeoA domain, but a closely related TroR protein from *Treponema denticola* has both the FeoA domain and an aspartyl residue at the position equivalent to Asp160 in ScaR (Figure 11 (*39*)). Looking farther afield, a related metalloregulator from *Deinococcus radiodurans* has an aspartyl residue at position 123 (*37*), replacing a cysteine, still consistent with the notion of a widely conserved metal-binding site among DtxR/MntR family members. Although it is possible that the observation of divalent metal ions in the secondary site of ScaR is an artifact of our crystallization conditions, the broad conservation of potential metal-binding residues at the appropriate positions across the DtxR/MntR family and the observation that ScaR binds multiple metal ions per subunit suggest that metal binding at this site fulfills a selected function.

Beyond the functional puzzle, the secondary site is somewhat surprising in its structure. The presence of a cysteinyl residue at position 123 is unusual for a Mn^{2+}-binding site. In a survey of manganese-binding sites among protein structures deposited in the Protein Data Bank in 2003 it was found that, of the 109 structures solved to 2.5 Å or better, only one protein, 3-deoxy-D-*arabino*-heptulosonate-7-phosphate (DHAP) synthase, contains a sulfur ligand, but there is evidence that this protein is Fe^{2+}-dependent *in vivo* (*50*, *51*). Notably, the ligand selection in DHAP synthase is identical to that in the secondary site of ScaR, with a cysteine, aspartate, glutamate, and histidine each contributing to metal binding. Assuming a functional role for this site, it is an open question as to whether it is designed to bind Mn^{2+} or some other metal ion under cellular conditions.

Thus, a number of unresolved issues remain with respect to the structural mechanism by which ScaR is activated to bind DNA by cognate effector ions. Future studies will be required to determine the functional role of the putative primary site and of the secondary metal-binding site. Also, the structural differences between ScaR and DtxR, including the stable dimer formed by apo-ScaR and the relatively fixed position of the FeoA domain in ScaR, indicate that the mechanisms of metal ion activation of these two proteins are distinct. Studies are under way to determine the functional roles of the FeoA domain of and the secondary metal-binding site.

REFERENCES

1. Jakubovics, N. S., and Jenkinson, H. F. (2001) Out of the iron age: new insights into the critical role of manganese homeostasis in bacteria. *Microbiology* (*Reading, U.K.*) *147*, 1709–1718.
2. Zaharik, M. L., and Finlay, B. B. (2004) Mn^{2+} and bacterial pathogenesis. *Front. Biosci. 9*, 1035–1042.
3. Papp-Wallace, K. M., and Maguire, M. E. (2007) Manganese transport and the role of manganese in virulence. *Annu. Rev. Microbiol. 60*, 187–209.
4. Kitten, T., Munro, C. L., Michalek, S. M., and Macrina, F. L. (2000) Genetic characterization of a *Streptococcus mutans* LraI family operon and role in virulence. *Infect. Immun. 68*, 4441–4451.
5. Andersen, R. N., Ganeshkumar, N., and Kolenbrander, P. E. (1993) Cloning of the *Streptococcus gordonii* PK488 gene, encoding an adhesin which mediates coaggregation with *Actinomyces naeslundii* PK606. *Infect. Immun. 61*, 981–987.
6. Kolenbrander, P. E., Andersen, R. N., Baker, R. A., and Jenkinson, H. F. (1998) The adhesion-associated *sca* operon in *Streptococcus gordonii* encodes an inducible high-affinity ABC transporter for Mn^{2+} uptake. *J. Bacteriol. 180*, 290–295.
7. Jakubovics, N. S., Smith, A. W., and Jenkinson, H. F. (2000) Expression of the virulence-related Sca (Mn^{2+}) permease in *Streptococcus gordonii* is regulated by a diphtheria toxin metallorepressor-like protein ScaR. *Mol. Microbiol. 38*, 140–153.
8. Bates, C. S., Toukoki, C., Neely, M. N., and Eichenbaum, Z. (2005) Characterization of MtsR, a new metal regulator in group A *Streptococcus*, involved in iron acquisition and virulence. *Infect. Immun. 73*, 5743–5753.
9. Johnston, J. W., Briles, D. E., Myers, L. E., and Hollingshead, S. K. (2006) Mn^{2+}-dependent regulation of multiple genes in *Streptococcus pneumoniae* through PsaR and the resultant impact on virulence. *Infect. Immun. 74*, 1174–1180.

10. Boyd, J., Oza, M. N., and Murphy, J. R. (1990) Molecular cloning and DNA sequence analysis of a diphtheria *tox* iron-dependent regulatory element (*dtxR*) from *Corynebacterium diphtheriae*. *Proc. Natl. Acad. Sci. U.S.A. 87*, 5968–5972.
11. Que, Q., and Helmann, J. D. (2000) Manganese homeostasis in *Bacillus subtilis* is regulated by MntR, a bifunctional regulator related to the diphtheria toxin repressor family of proteins. *Mol. Microbiol. 35*, 1454–1468.
12. Qiu, X., Pohl, E., Holmes, R. K., and Hol, W. G. J. (1996) High-resolution structure of the diphtheria toxin repressor complexed with cobalt and manganese reveals an SH3-like third domain and suggests a possible role of phosphate as Co-corepressor. *Biochemistry 35*, 12292–12302.
13. Spiering, M. M., Ringe, D., Murphy, J. R., and Marletta, M. A. (2003) Metal stoichiometry and functional studies of the diphtheria toxin repressor. *Proc. Natl. Acad. Sci. U.S.A. 100*, 3808–3813.
14. Pohl, E., Holmes, R. K., and Hol, W. G. J. (1999) Crystal structure of the iron-dependent regulator (IdeR) from *Mycobacterium tuberculosis* shows both metal binding sites fully occupied. *J. Mol. Biol. 285*, 1145–1156.
15. Glasfeld, A., Guedon, E., Helmann, J. D., and Brennan, R. G. (2003) Structure of the manganese-bound transporter of *Bacillus subtilis*. *Nat. Struct. Biol. 10*, 562–657.
16. Kliegman, J. I., Griner, S. L., Helmann, J. D., Brennan, R. G., and Glasfeld, A. (2006) Structural basis for the metal-selective activation of the manganese transport regulator of *Bacillus subtilis*. *Biochemistry 45*, 3493–3505.
17. Guedon, E., and Helmann, J. D. (2003) Origins of metal ion selectivity in the DtxR/MntR family of metalloregulators. *Mol. Microbiol. 48*, 495–506.
18. White, A., Ding, X., vanderSpek, J. C., Murphy, J. R., and Ringe, D. (1998) Structure of the metal-ion-activated diphtheria toxin repressor/tox operator complex. *Nature 394*, 502–506.
19. Lundblad, J. R., Laurance, M., and Goodman, R. H. (1996) Fluorescence polarization analysis of protein-DNA and protein-protein interactions. *Mol. Endocrinol. 10*, 607–612.
20. Kumaraswami, M., Schuman, J. T., Seo, S. M., Kaatz, G. W., and Brennan, R. G. (2009) Structural and biochemical characterization of MepR, a multidrug binding transcription regulator of the *Staphylococcus aureus* multidrug efflux pump MepA. *Nucleic Acids Res. 37*, 396–401.
21. Doublié, S. (1997) Preparation of selenomethionyl proteins for phase determination. *Methods Enzymol. 276*, 523–529.
22. Leslie, A. G. W. (1992) Recent changes to the MOSFLM package for processing film and image plate data, Joint CCP4 + ESF-EAMCB Newsletter on Protein Crystallography 26 .
23. Pflugrath, J. W. (1999) The finer things in X-ray diffraction data collection. *Acta Crystallogr., Sect. D: Biol. Crystallogr. 55*, 1718–1725.
24. Terwilliger, T. C., and Berendzen, J. (1999) Automated MAD and MIR structure solution. *Acta Crystallogr., Sect. D: Biol. Crystallogr. 55*, 849–861.
25. Brunger, A. T., Adams, P. D., Clore, G. M., Delano, W. L., Gros, P., Grosse-Kunstleve, R. W., Jiang, J.-S., Kuszewski, J., Nilges, M., Pannu, N. S., Read, R. J., Rice, L. M., Simonson, T., and Warren, G. L. (1998) Crystallography & NMR system: a new software suite for macromolecular structure determination. *Acta Crystallogr., Sect. D: Biol. Crystallogr. 54*, 905–921.
26. Murshudov, G. N., Vagin, A. A., and Dodson, E. J. (1997) Refinement of macromolecular structures by the maximum-likelihood method. *Acta Crystallogr., Sect. D: Biol. Crystallogr. 54*, 1285–1294.
27. Collaborative Computational Project, Number 4 (1994) The CCP4 suite: programs for protein crystallography. *Acta Crystallogr., Sect. D: Biol. Crystallogr. 50*, 760–763.
28. Adams, P. D., Grosse-Kunstleve, R. W., Hung, L.-W., Ioerger, T. R., McCoy, A. J., Moriarty, N. W., Read, R. J., Sacchettini, J. C., Sauter, N. K., and Terwilliger, T. C. (2002) PHENIX: building new software for automated crystallographic structure determination. *Acta Crystallogr., Sect. D: Biol. Crystallogr. 58*, 1948–1954.
29. Painter, J., and Merritt, E. A. (2006) Optimal description of a protein structure in terms of multiple groups undergoing TLS motion. *Acta Crystallogr., Sect. D: Biol. Crystallogr. 62*, 439–450.
30. Laskowski, R. A., MacArthur, M. W., Moss, D. S., and Thornton, J. M. (1993) PROCHECK: a program to check the stereochemical quality of protein structures. *J. Appl. Crystallogr. 26*, 283–291.
31. Feese, M. D., Ingason, B. P., Goranson-Siekierke, J., Holmes, R. K., and Hol, W. G. J. (2001) Crystal structure of the iron-dependent regulator from *Mycobacterium tuberculosis* at 2.0 Å resolution reveals the src homology domain 3-like fold and metal binding function of the third domain. *J. Biol. Chem. 276*, 5959–5966.
32. Kammler, M., Schon, C., and Hantke, K. (1993) Characterization of the ferrous iron uptake system of *Escherichia coli*. *J. Bacteriol. 175*, 6212–6219.
33. Finn, R. D., Tate, J., Mistry, J., Coggill, P. C., Sammut1, S. J., Hotz, H.-R., Ceric, G., Forslund, K., Eddy, S. R., Sonnhammer, E. L. L., and Bateman, A. (2008) The Pfam protein families database. *Nucleic Acids Res. 36*, D281–D288.
34. Brennan, R. G. (1993) The winged-helix DNA-binding motif: another helix-turn-helix takeoff. *Cell 74*, 773–776.
35. DeWitt, M. A., Kliegman, J. I., Helmann, J. D., Brennan, R. G., Farrens, D. L., and Glasfeld, A. (2007) The conformations of the metal-free form of the manganese transport regulator of *Bacillus subtilis*. *J. Mol. Biol. 365*, 1257–1265.
36. Pohl, E., Holmes, R. K., and Hol, W. G. J. (1998) Motion of the DNA-binding domain with respect to the core of the diphtheria toxin repressor (DtxR) revealed in the crystal structures of apo- and holo-DtxR. *J. Biol. Chem. 273*, 22420–22427.
37. Cole, S. T., Brosch, B., Parkhill, J., Garnier, T., Churcher, C., Harris, D., Gordon, S. V., Eiglmeier, K., Gas, S., Barry, C. E., Tekaia, F., Badcock, K., Basham, D., Brown, D., Chillingworth, R., Connor, R., Davies, K., Devlin, T., Feltwell, S., Gentles1, N., Hamlin, S., Holroyd, T., Hornsby, T., Jagels, K., Krogh, A., McLean, J., Moule, S., Murphy, L., Oliver, J., Osborne, K., Quail, M. A., Rajandream, M.-A., Rogers, J., Rutter, S., Seeger, K., Skelton, J., Squares, R., Squares, S., Sulston, J. E., Taylor, K., Whitehead, S., and Barrell, B. G. (1998) Deciphering the biology of *Mycobacterium tuberculosis* from the complete genome sequence. *Nature 393*, 537–544.
38. White, O., Eisen, J. A., and Heidelberg, John F.; et al. (1999) Genome sequence of the radioresistant bacterium *Deinococcus radiodurans* R1. *Science 286*, 1571–1577.
39. Brett, P. J., Burtnick, M. N., Fenno, J. C., and Gherardini, F. C. (2008) *Treponema denticola* TroR is a manganese- and iron-dependent transcriptional repressor. *Mol. Microbiol. 70*, 396–409.
40. Langlais, M., Tajmir-Riahi, H. A., and Savoie, R. (1990) Raman spectroscopic study of the effects of Ca^{2+}, Mg^{2+}, Zn^{2+} and Cd^{2+} ions on calf thymus DNA: binding sites and conformational changes. *Biopolymers 30*, 743–752.
41. Kejnovsky, E., and Kypr, J. (1998) Millimolar concentrations of zinc and other cations cause sedimentation of DNA. *Nucleic Acids Res. 23*, 5295–5299.
42. Kloosterman, T., Witwicki, R. M., van der Kooi-Pol, M. M., Bijlsma, J. J., and Kuipers, O. P. (2008) Opposite effects of Mn^{2+} and Zn^{2+} on the PsaR-mediated expression of the virulence genes *pcpA*, *prtA* and *psaBCA* of *Streptococcus pneumoniae*. *J. Bacteriol. 190*, 5382–5393.
43. Tao, X., and Murphy, J. R. (1992) Binding of the metalloregulatory protein DtxR to the diphtheria *tox* operator requires a divalent heavy metal ion and protects the palindromic sequence from DNase I digestion. *J. Biol. Chem. 267*, 21761–21764.
44. Schmitt, M. P., and Holmes, R. K. (1993) Analysis of diphtheria toxin repressor-operator interactions and characterization of a mutant repressor with decreased binding activity for divalent metals. *Mol. Microbiol. 9*, 173–181.
45. Waldron, K. J., Rutherford, J. C., Ford, D., and Robinson, N. J. (2009) Metalloproteins and metal sensing. *Nature 460*, 823–830.
46. Qiu, X., Verlinde, C. L., Zhang, S., Schmitt, M. P., Holmes, R. K., and Hol, W. G. L. (1995) Three-dimensional structure of the diphtheria toxin repressor in complex with divalent cation co-repressors. *Structure 3*, 87–100.
47. Rangachari, V., Marin, V., Bienkiewicz, E. A., Semavina, M., Guerrero, L., Love, J. F., Murphy, J. R., and Logan, T. M. (2005) Sequence of ligand binding and structure change in the diphtheria toxin repressor upon activation by divalent transition metals. *Biochemistry 44*, 5672–5682.
48. D'Aquino, J. A., Tetenbaum-Novatt, J., White, A., Berkovitch, F., and Ringe, D. (2005) Mechanism of metal ion activation of the diphtheria toxin repressor DtxR. *Proc. Natl. Acad. Sci. U.S.A. 102*, 18408–18413.
49. Wylie, G. P., Rangachari, V., Bienkiewicz, E. A., Marin, V., Bhattacharya, N., Love, J. F., Murphy, J. R., and Logan, T. M. (2005) Prolylpeptide binding by the prokaryotic SH3-like domain of the diphtheria toxin repressor: a regulatory switch. *Biochemistry 44*, 40–51.
50. Harding, M. M. (2004) The architecture of metal coordination groups in proteins. *Acta Crystallogr., Sect. D: Biol. Crystallogr. 60*, 849–859.
51. Waner, T., Shumilin, I. A., Bauerle, R., and Kretsinger, R. H. (2001) Structure of 3-deoxy-D-arabino-heptulosonate-7-phosphate synthase from *Escherichia coli*: comparison of the Mn^{2+} 2-phosphoglycolate and the Pb^{2+} 2-phosphoenolpyruvate complexes and implications for catalysis. *J. Mol. Biol. 301*, 389–399.